

U.S. DEPARTMENT OF THE INTERIOR

U.S. GEOLOGICAL SURVEY

**Heat-Flow Measurements
in the Vicinity of the Hayward Fault, California**

by

Colin F. Williams and S. Peter Galanis, Jr.¹



Open-File Report 94-692

This report is preliminary and has not been reviewed for conformity with U.S. Geological Survey editorial standards or with the North American Stratigraphic Code. Any use of trade, firm, or product names is for descriptive purposes only and does not constitute endorsement by the U.S. Government.

1994

¹U.S. Geological Survey, Menlo Park, CA 94025

Contents

	<u>page</u>
Abstract	2
Introduction	3
Drilling and Completion Operations	5
Temperature and Thermal Conductivity Data	6
Heat Flow	7
Conclusions23
Tables26
Appendix33
References35

ABSTRACT

In 1991 and 1992, temperature and thermal conductivity data were acquired from five borehole strainmeter exploratory pilot holes and one borehole strainmeter installation hole drilled near the southern segment of the Hayward fault. The locations of these six holes (Lake Chabot, Walpert Ridge above Niles Canyon, Coyote Hills, Garin Park, and Sunol Ridge) cover a 20 km by 30 km gap in existing heat flow data between the southern San Francisco Peninsula segment of the San Andreas fault and the northern segment of the Hayward fault. Although thermal disturbances due to locally rugged topography and shallow groundwater flow are substantial at all but the Coyote Hills site, reliable conductive heat flow measurements have been obtained from four of the six holes. Heat flow is 83.3 ± 6.6 mW/m² at Lake Chabot, 80.0 ± 15.0 mW/m² at Niles Canyon (two holes), and 96.3 ± 2.5 mW/m² at Coyote Hills. Incomplete data suggest that heat flow is greater than 80 mW/m² at Garin Park. These new values are similar to an 84 mW/m² value measured in the Berkeley Hills to the north and an average of 89.2 mW/m² from six sites on the southern San Francisco Peninsula. This places the Hayward fault well within the region of elevated heat flow that characterizes most of the California Coast Ranges. In addition, if these measurements reflect near steady-state thermal conditions at depth, temperatures in the crust and upper mantle beneath the Hayward fault are indistinguishable from those beneath the Peninsula segment of the San Andreas fault.

INTRODUCTION

As part of a U.S. Geological Survey program to install borehole strainmeters near the Hayward fault (Johnston et al., 1992), exploratory pilot holes were drilled at seven sites along the southern segment of the fault in order to determine the appropriate locations and depths for eventual installation of the strainmeters. At five of these sites, the pilot holes were completed with tubing cemented in place, providing access for continuing subsurface studies after the completion of drilling. Subsurface temperatures in these holes were recorded by the USGS Geothermal Studies Project in the weeks and months following completion to determine equilibrium geothermal gradients. In addition, core, cuttings, and surface samples were collected for thermal conductivity measurements and then combined with the geothermal gradient information in calculations of subsurface heat flow.

This report summarizes these measurements and the resulting heat-flow determinations from five of the pilot holes. Until the acquisition of these new data, heat flow information in the vicinity of the Hayward fault was limited to a single measurement near the UC Berkeley campus (Figure 1). The 84 mW/m^2 value measured at this site is consistent with the relatively high heat flow measured west of the San Francisco Bay and elsewhere in the California Coast Ranges (Lachenbruch and Sass, 1980). Heat flow decreases to the east of the Calaveras Fault in the transition between the Coast Ranges and the Central Valley. The previously published data are too sparse for determining the spatial variation of heat flow within this transition region. Consequently, the new data discussed below provide valuable information on the variation in heat flow both along the Hayward fault and in the region between the Hayward and Calaveras faults. This thermal information can be extrapolated to depth in order to estimate crustal temperatures and, with some additional information regarding lithology and strain rate, the crustal rheology of this complex plate boundary.

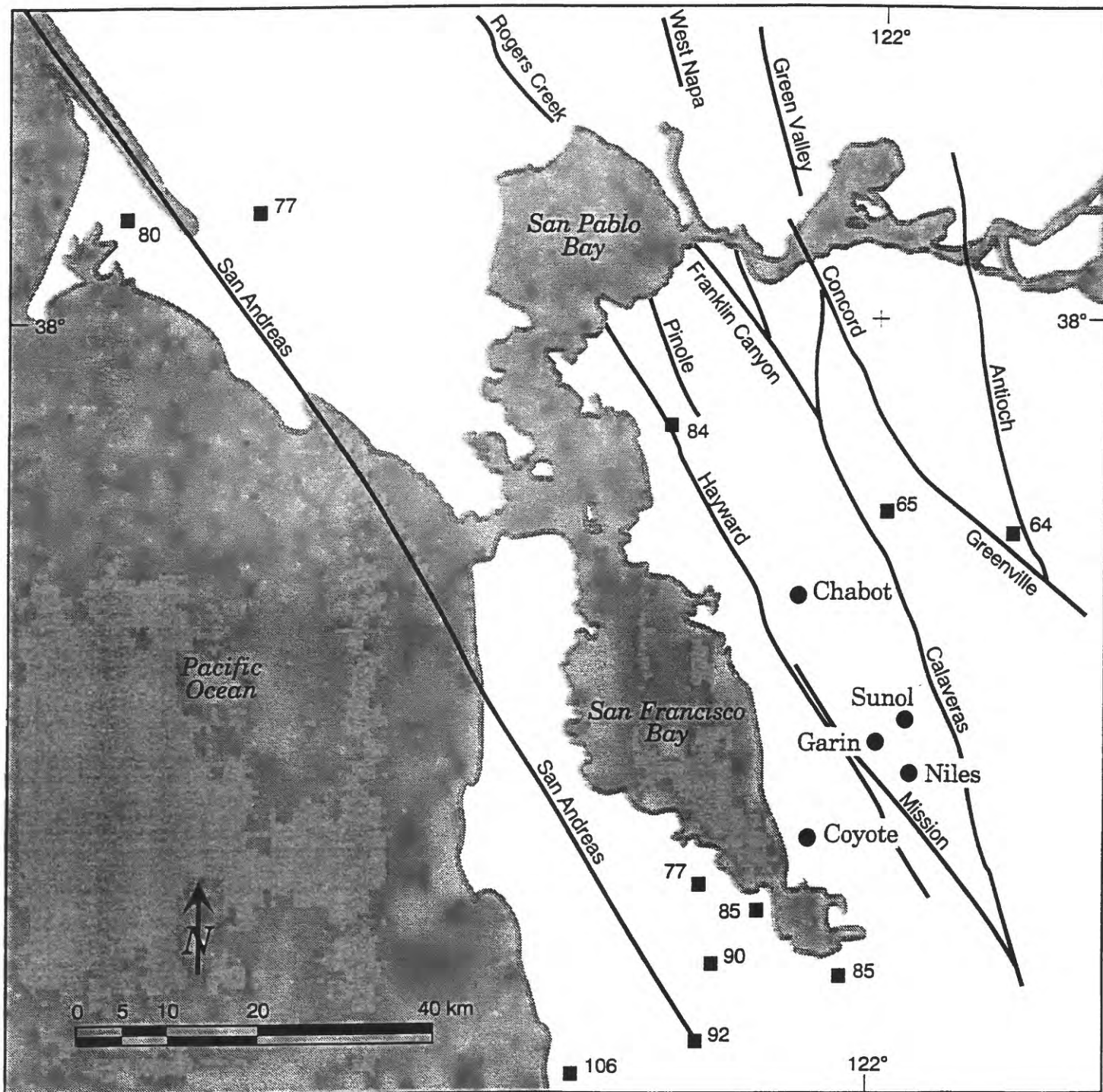


Figure 1 - Location map showing previously published heat-flow measurements in the San Francisco Bay area, the new sites described in this report, and major faults. Note that the 65 mW/m^2 value located just east of the Calaveras fault is a revision of the value reported by Lachenbruch and Sass (1980).

DRILLING AND COMPLETION OPERATIONS

The six holes discussed in this report were drilled in the period from September, 1991 to September, 1992. Five of the holes are pilot holes drilled prior to strainmeter installation, and the sixth is one of the subsequently drilled strainmeter holes. These small diameter (5.25 inches or 13.3 cm) pilot holes were drilled to identify the appropriate location and depth for strainmeter emplacement. Because strainmeters must be installed in cased holes and local requirements are for a minimum of 2 inches of cement outside of the casing, a relatively large diameter hole (11 inches or 27.9 cm) must be drilled into a competent rock formation for each strainmeter. Pilot holes are a cost-effective means of investigating subsurface conditions before incurring the substantial cost of drilling the strainmeter holes.

These five pilot holes were completed as heat-flow holes in the manner outlined by Moses and Sass (1979). Most of the drilling was accomplished with the rotary technique using air as the drilling fluid, although difficult drilling conditions often made it necessary to switch to drilling mud before the target depth could be reached. Chip samples were collected at 6 meter (20 foot) intervals and spot cores were taken at target depths for strainmeter installation (typically > 120 meters). Upon completion of drilling, 3.2 cm (1.25 inch) diameter tubing was lowered into each hole and cemented in place. Although plans called for cement lining the hole annulus from total depth to the surface, some of the holes are only partially cemented (see discussion below).

For each hole, open hole logs were run before the tubing was cemented in place. These logs included caliper, gamma ray, resistivity, spontaneous potential, and borehole televiewer measurements, although adverse hole conditions and other operational problems limited the success of these logging efforts. Subsurface temperature logs were recorded immediately after completion and at irregular intervals over the following year. The temperature data presented in this report represent near-equilibrium measurements recorded by the last series of logs.

The names, locations, and depths of the holes discussed in this report are summarized in Table 1, and the locations are shown in Figure 1. Except for the Coyote Hills site, the holes were located in the hills east of the Hayward Fault within sandstones, shales and conglomerates of the Cretaceous Panoche Formation as identified by Dibblee (1980a,b). In general, massive

sandstone predominates, although shale layers of varying thickness are common and correlate with intervals of hole instability. Formation dips are variable but are consistent in magnitude with the surface dips mapped by Dibblee (1980a,b). Fracturing is common in the cores from the Niles and Sunol sites, a result confirmed by borehole televiewer logs (J. Svitek, written comm., 1992).

The Coyote Hills hole was drilled into the Jurassic-Cretaceous Franciscan Formation (Snetsinger, 1976). The Franciscan Formation in the Coyote Hills is predominantly composed of greenstone (60%) with tightly folded beds of chert, graywacke and argillite making up the remainder (Snetsinger, 1976), although the drillhole penetrated graywacke and argillite exclusively. Samples show common shear fabrics and fracturing, with most fractures filled with calcite cement.

TEMPERATURE AND THERMAL CONDUCTIVITY DATA

Temperature profiles were recorded for each hole immediately after the end of drilling and in the following months. The final temperature logs are essentially equilibrium values except for the profiles from the Garin Park (GAR2). GAR1, the pilot hole, was partially plugged with cement, so a non-equilibrium profile was obtained from GAR2, the strainmeter hole, before installation of the strainmeter. Temperature profiles were corrected for steady-state topography using the method of Birch (1950). Thermal conductivities were measured on disks cut from core samples in a "divided-bar" apparatus (Sass et al., 1971). Whenever possible, measurements were made of both the vertical and horizontal conductivity in order to establish the degree of thermal conductivity anisotropy. The thermal conductivity of cuttings samples was also measured in the divided-bar using the chip cell technique developed by Sass, Lachenbruch, and Munroe (1971). This technique yields the rock matrix thermal conductivity, so the bulk rock thermal conductivity was estimated by applying a geometric mean model for the thermal conductivity of a porous medium,

$$\lambda_b = \lambda_f^\phi \cdot \lambda_m^{1-\phi} \quad (1)$$

where λ_b is the bulk rock conductivity, λ_f is the water conductivity, λ_m is the rock matrix conductivity, and ϕ is the fractional porosity. Porosity was estimated from the average values measured on core samples from each well. Because there is substantial variability in the temperature profiles and thermal conductivities, each site is discussed separately.

HEAT FLOW

LAKE CHABOT #1 (CHA1)

This hole was drilled to a depth of 151 meters (494 feet) at a site located approximately 1.7 km northeast of Lake Chabot and 3.2 km northeast of the Hayward Fault. As described in Table 2, the hole penetrated sandstone and shale of the Panoche Formation on the western limb of the "Niles Syncline" mapped by Dibblee (1980a,b). Drilling of this hole was hampered by the presence of an unstable shale layer at 104 meters. The instability of this layer (possibly a permeable, bedding-plane fault contact - see below) precluded the acquisition of open hole logging data over most of the drilled interval but did not prevent the installation of tubing to the bottom of the hole. Dips at nearby surface outcrops range from 45 to 60°, values consistent with the 55° dips measured in the massive sandstone cored from 140 to 151 meters (Table 2).

Temperature, temperature gradient, and thermal conductivity data from CHA1 are shown in Figure 2. The primary feature in the temperature log is a decrease in the vertical temperature gradient at 104 meters that does not correspond to a change in the thermal conductivity. After correcting for topography, heat flow in the interval from 70 meters (top of cement) to 100 meters averages 112.1 +/- 4.7 mW/m². Heat flow in the interval from 110 meters to 151 meters is 83.3 +/- 3.5 mW/m². The sharpness of the gradient break, the linearity of the temperature profile, and the correspondence of the gradient break with the interval of hole instability are consistent with two possible explanations.

First, warm groundwater flowing upward along a fault/fracture plane intersecting the hole at 104 meters could produce higher heat flow in the interval above the intersection. However, the Chabot site is perched near the top of a hill approximately 185 meters above Lake Chabot. In this environment, it is difficult, if not impossible, to develop the hydraulic potentials necessary to drive water uphill from the nearby lake. Second, this possible fault plane could

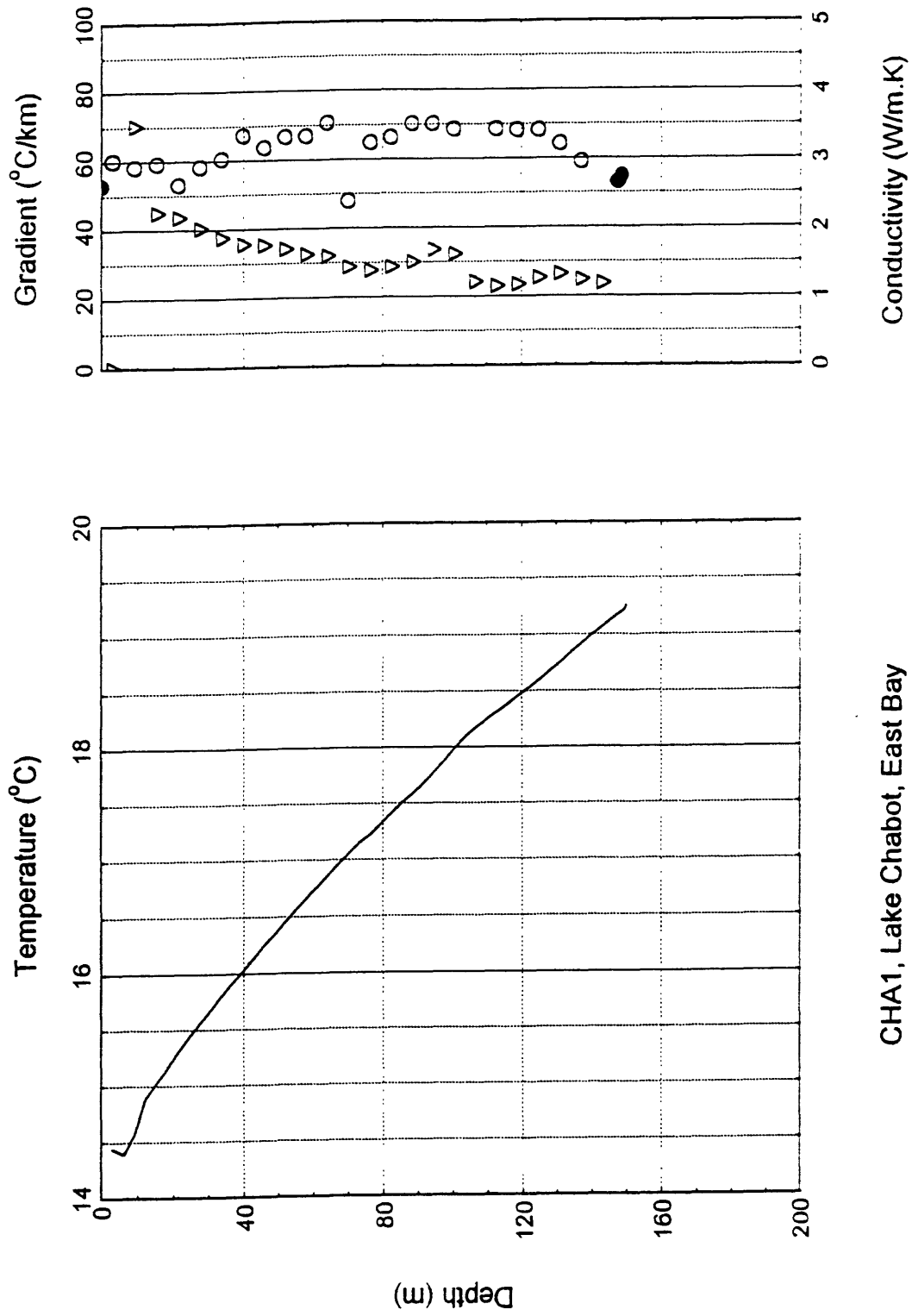


Figure 2 - Temperature (solid line), vertical temperature gradient (open triangles), bulk thermal conductivity measured on core samples (solid circles) and bulk conductivity determined from cuttings samples (open circles) for CHA1.

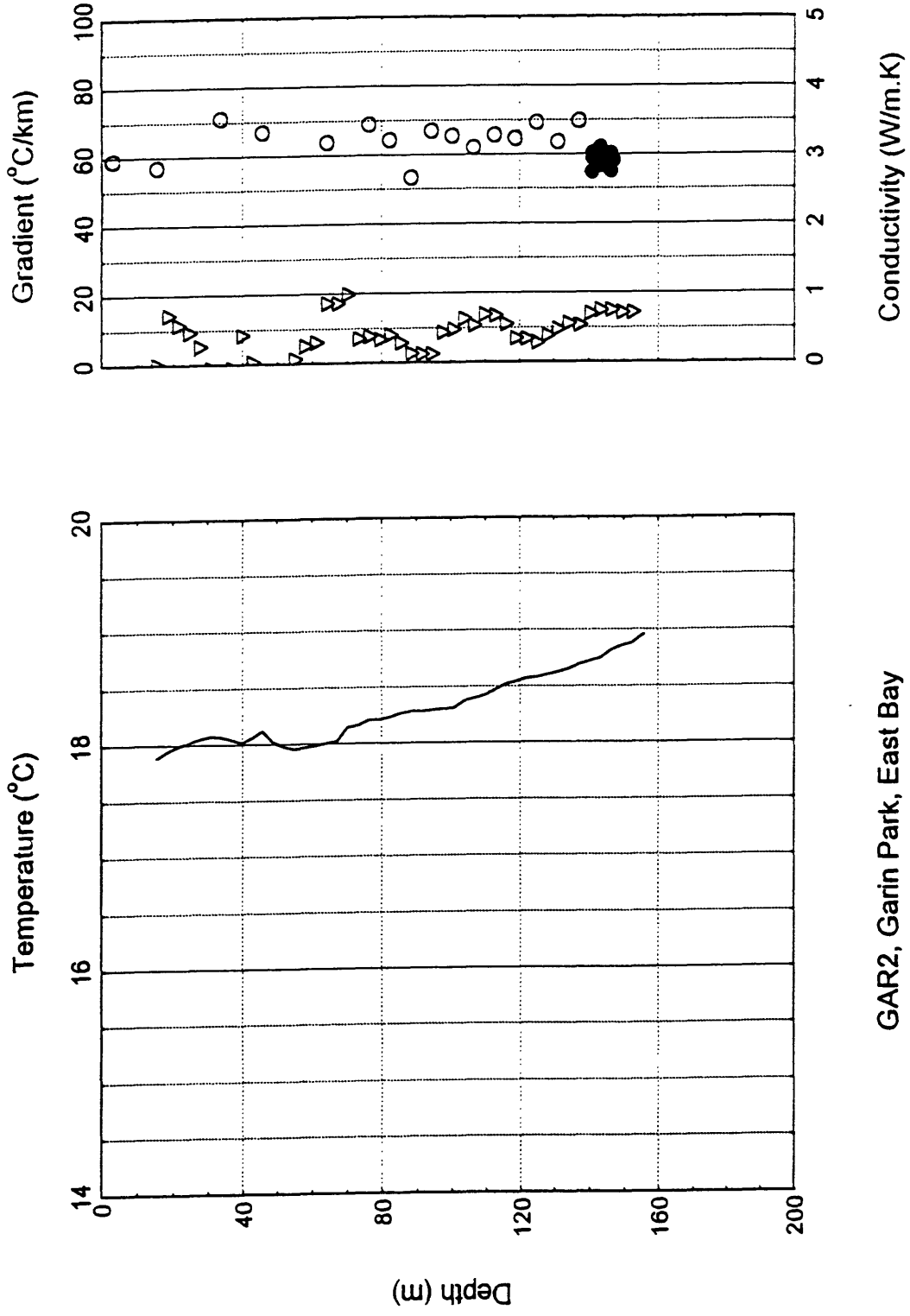
juxtapose sedimentary layers of differing dip, resulting in a discontinuity in thermal conductivity. The bulk conductivities derived from chip measurements are based on an assumption of conductivity isotropy. If, for this formation, the component of conductivity parallel to the bedding plane is substantially higher than the component of conductivity perpendicular to the bedding plane and the sedimentary layers above the fault plane are subhorizontal, the observed gradient change would result. Heat flow would be constant with depth at approximately 83 mW/m² (the value derived from measurements on both core samples with the 55° dip and adjacent cuttings samples). However, oriented conductivity measurements from the Niles #1 and #2 wells, which penetrated a similar sedimentary sequence in the Niles syncline approximately 15 kilometers to the south (Figure 1), are essentially isotropic. In addition, surface dips measured at the Chabot site by the authors and by Dibblee (1980a) match those measured on the core from 140 to 151 meters. If dips vary downhole, they must shallow in the first 200 feet and then steepen abruptly at the fault contact.

Whether the apparent vertical variation in heat flow is due to groundwater flow or thermal conductivity anisotropy, the heat flow measured below a depth of 110 meters would be relatively undisturbed. Consequently, the 83.3 mW/m² measured from 110 to 151 meters is presented in Table 6 as the appropriate average value for this site.

GARIN PARK #2 (GAR2) -

This hole was drilled to a depth of 156 meters (510 feet) at a site located approximately 3 kilometers northeast of the Hayward Fault (Figure 1). Pump failure left the pilot hole (GAR1) plugged with cement at 78 meters, so temperature data were recorded in the subsequent strainmeter hole (GAR2; Figure 3). Unfortunately, GAR2 was available for a limited time after drilling, and the temperature profile shown in Figure 3 does not represent equilibrium conditions.

There are two additional problems with the Garin Park site. First, its location at the edge of a ridge approximately 200 meters high and sloping off to the west at an angle of 30 degrees introduces a two-dimensional topographic disturbance that reduces conductive heat flow at this site by at least 50% and perhaps as much as 70% (see Lachenbruch, 1969 for a complete discussion of two-dimensional topographic corrections to surface heat flow). Second, surface



GAR2, Garin Park, East Bay

Figure 3 - Temperature (solid line), vertical temperature gradient (open triangles), bulk thermal conductivity measured on core samples (solid circles) and bulk conductivity determined from cuttings samples (open circles) for GAR2.

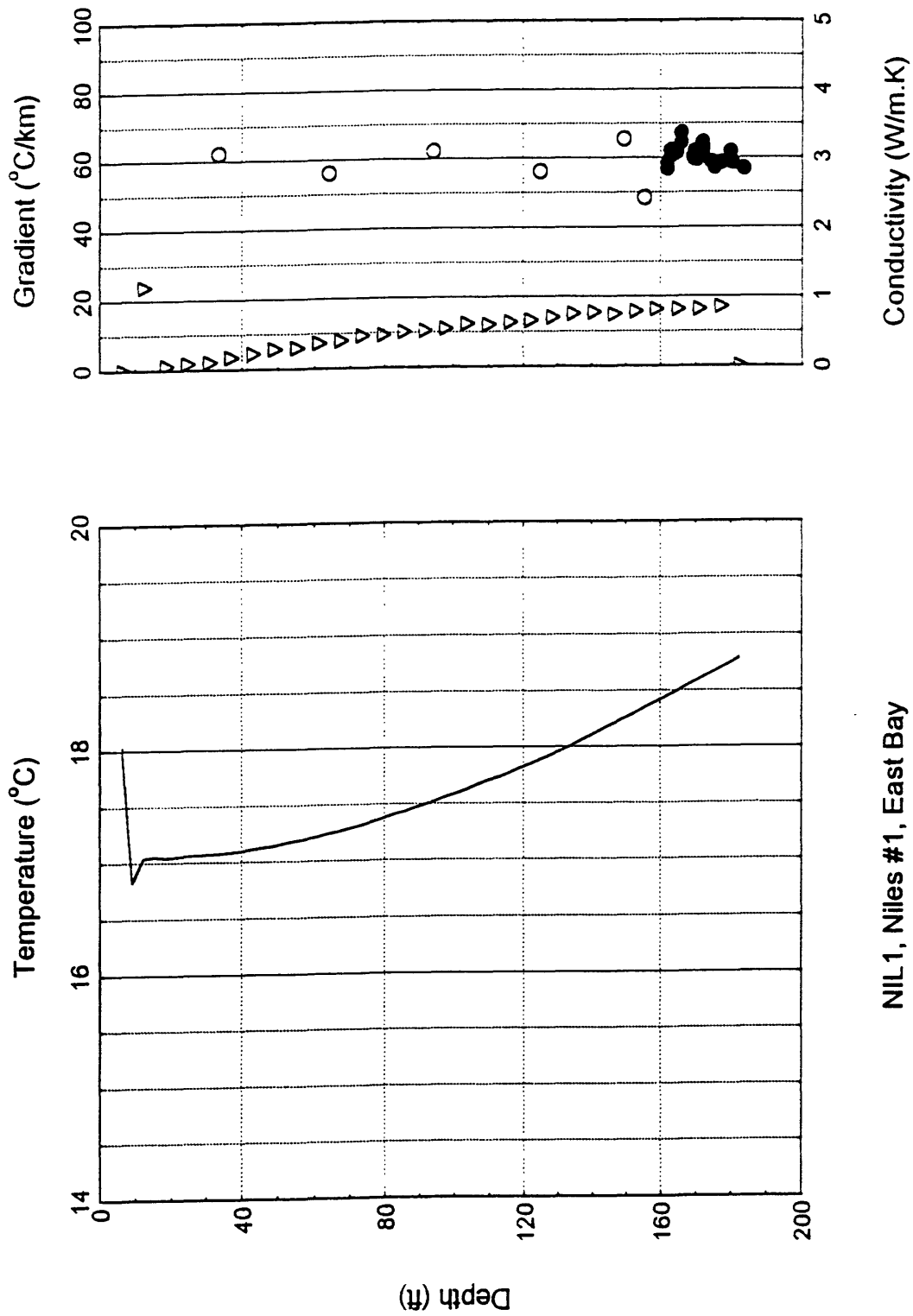
springs near the hole and reversals in the temperature log suggest that downslope groundwater flow may also reduce heat flow at this site. The measured heat flow in the cored section of the hole (140 to 148 meters) is approximately 40 mW/m² (Gradient = 14.7 °C/km; Conductivity = 2.9 W/m.K), so the topographically "corrected" heat flow, without regard for fluid flow, lies in the range of 80 to 140 mW/m². However, the uncertainties associated with this correction and unknown effects of disequilibrium on the measured temperatures leave this result highly suspect. Consequently, the estimated heat flow for the Garin Park site, although listed in Table 6, has not been included with the other values in the final heat flow map.

NILES #1 and #2 (NIL1, NIL2) -

These two holes were drilled at separate sites located approximately 1.7 kilometers apart near the crest of Walpert Ridge north of Niles Canyon (Figure 1). NIL1 reached a depth of 184 meters, and NIL2 reached a depth of 168 meters. Lithologic data from the two holes are summarized in Tables 3 and 4, and the thermal data are plotted in Figures 4 and 5. As at the Lake Chabot site, the sedimentary rocks penetrated at the Niles sites have dips in the range of 35 to 70°. A significant difference between Niles and Chabot is the pervasive shear fabric found in both cores and cuttings. The intense fracturing visible in the core from the lower 25 meters of NIL1 (Table 2) is also found in the borehole televiewer log from the upper section of the hole (J. Svitek, written comm., 1992).

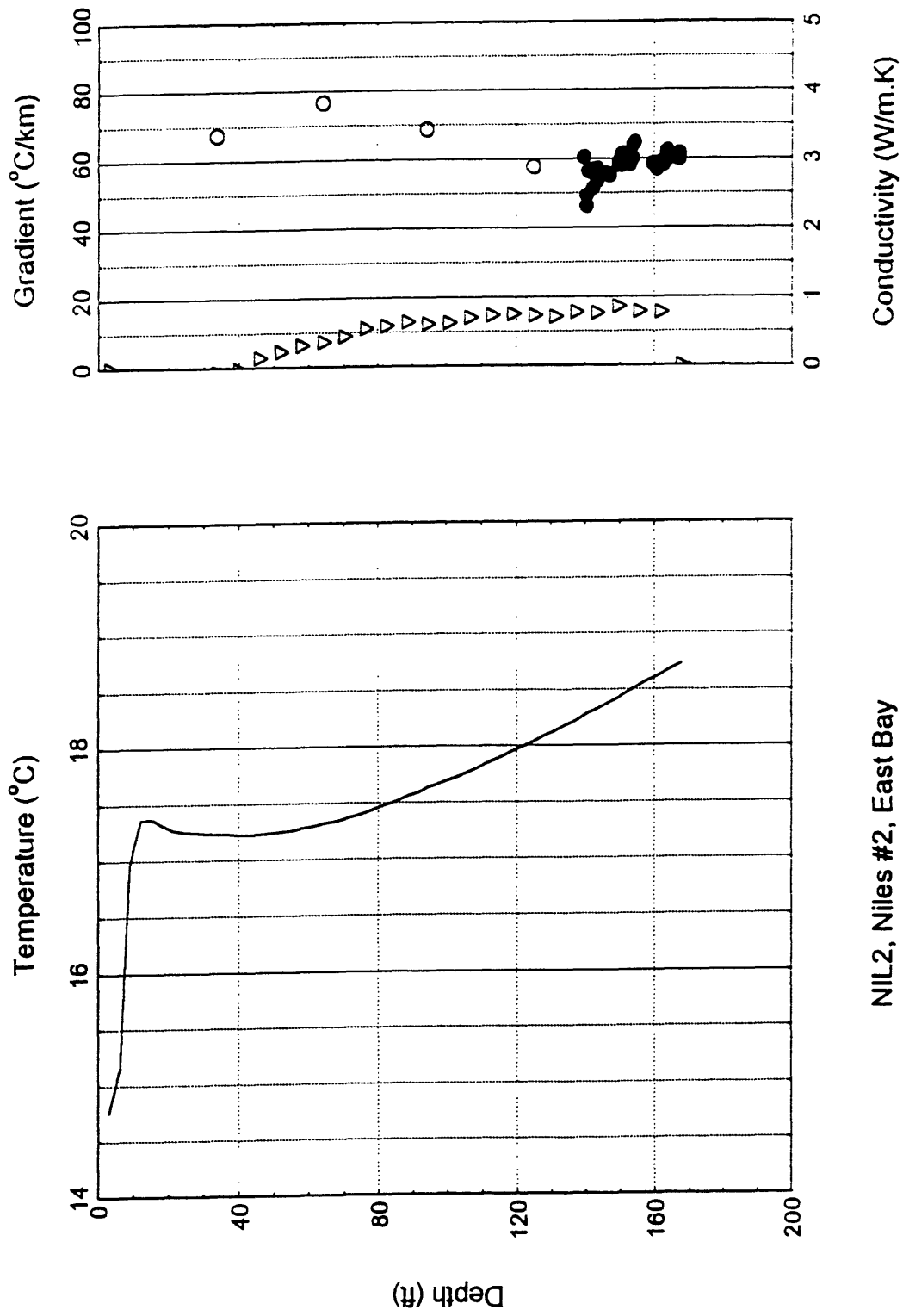
Thermal conductivities were measured on both cores and cuttings. The abundant core from NIL1 and NIL2 provided an opportunity to measure the thermal conductivity anisotropy. For NIL1, the average of 21 vertical divided-bar measurements is 3.047 +/- 0.055 W/m.K (the uncertainty is the 95% confidence limit). The average of 13 horizontal measurements is 3.075 +/- 0.100. For NIL2, the average of 20 vertical measurements is 2.912 +/- 0.095, and the average of 12 horizontal measurements is 2.899 +/- 0.100. Within the repeatability of the technique (+/- 2%) and the statistical uncertainty of the measurements, the core recovered from the two Niles holes is thermally isotropic.

The temperature profiles for NIL1 and NIL2 show a characteristic curvature in the upper 90 to 120 meters that appears to flatten out near the bottom of each hole to a gradient of approximately 17 °C/km (Table 6). Topographic corrections did not remove this curvature, and



NIL1, Niles #1, East Bay

Figure 4 - Temperature (solid line), vertical temperature gradient (open triangles), bulk thermal conductivity measured on core samples (solid circles) and bulk conductivity determined from cuttings samples (open circles) for NIL1.



NIL2, Niles #2, East Bay

Figure 5 - Temperature (solid line), vertical temperature gradient (open triangles), bulk thermal conductivity measured on core samples (solid circles) and bulk conductivity determined from cuttings samples (open circles) for NIL2.

the relatively constant thermal conductivity confirms that the curvature reflects a change in the vertical component of conductive heat flow. This concave-upward curvature in temperature is characteristic of both the transient effects of increasing surface temperature (e.g. Lachenbruch and Marshall, 1986) and downward groundwater flow (e.g. Bredehoeft and Papadopoulos, 1965). Although both processes have similar effects on the shape of the subsurface temperature profile, they have different implications for the background conductive heat flow.

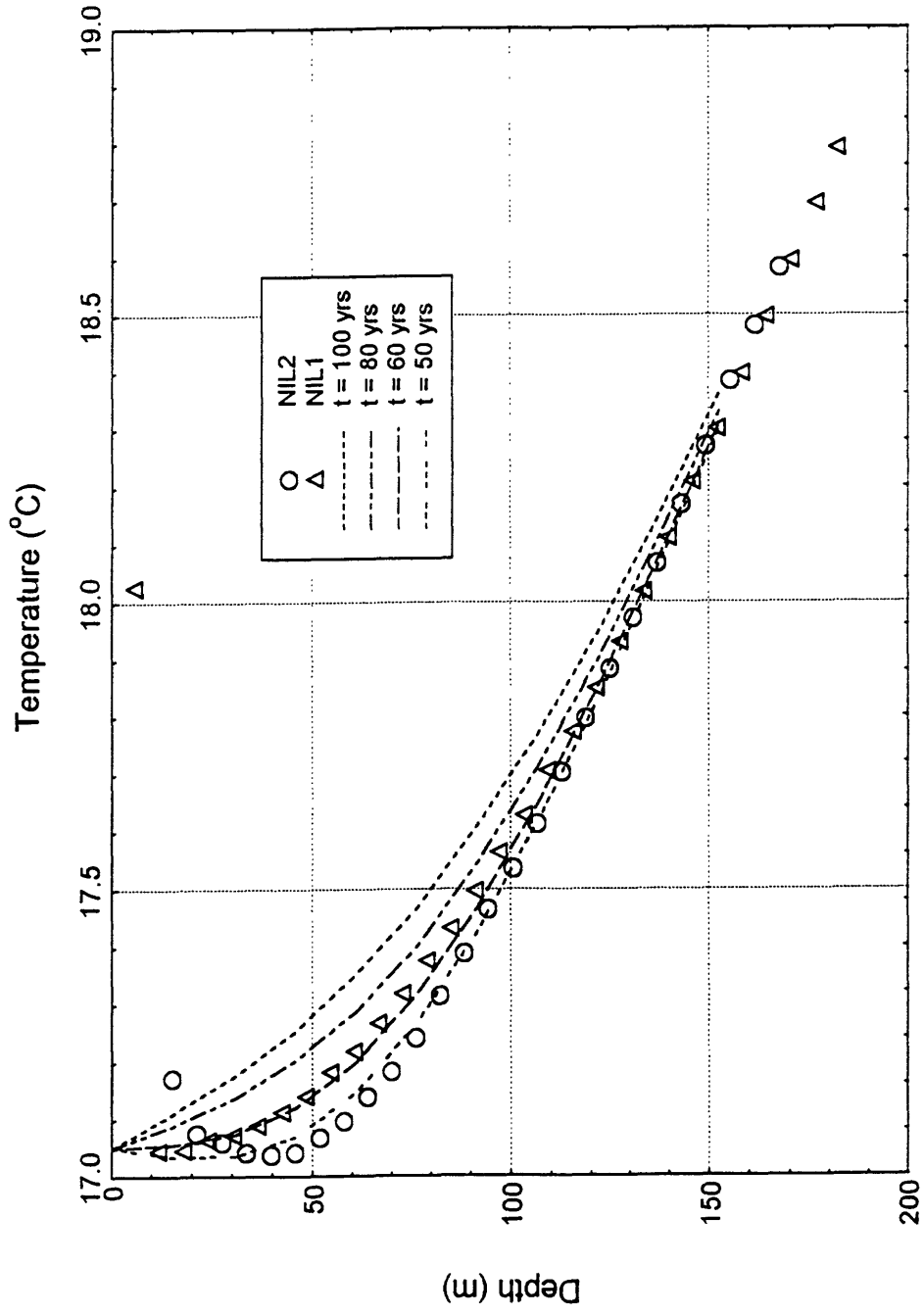
The possible effects of changing surface temperature are easily examined by considering a simple step change in temperature, ΔT , on the surface ($z = 0$) of a half-space at time $t=0$. The subsequent subsurface temperature profile is given by

$$T(z,t) = \Delta T \cdot \text{erfc}\left(\frac{z}{2\sqrt{\alpha t}}\right) \quad (2)$$

(e.g. Carslaw and Jaeger, 1959) where $\text{erfc}()$ is the complementary error function and α is the thermal diffusivity. This solution, with $\alpha = 1 \times 10^{-6} \text{ m}^2/\text{s}$, is compared to the data from NIL1 and NIL2 in Figure 6, where the apparent background geothermal gradient and equilibrium surface temperature have been added to the solution from equation (2). The data are well-matched by $\Delta T = 1.25 \text{ }^\circ\text{C}$ at a time 50 to 60 years before present. (Note that this analysis is only approximate and is not intended for use as a formal inversion.) The effects of this temperature change on the vertical temperature gradient decay with depth according to the derivative of Equation (2),

$$\frac{\partial T}{\partial z} = \frac{-\Delta T}{\sqrt{\pi \alpha t}} \cdot \exp\left(-\frac{z^2}{4\alpha t}\right) \quad (3)$$

For an event 60 years old, the gradient effect is less than $1 \text{ }^\circ\text{C}/\text{km}$ at a depth of 150 meters. Consequently, if the observed curvature is purely an effect of increasing surface temperature,



NIL1 & NIL2 - Effect of change in surface T at time t

Figure 6 - Temperature versus depth for NIL1 and NIL2 compared with profiles that would result from a 1.25 °C step increase in surface temperature at the specified times.

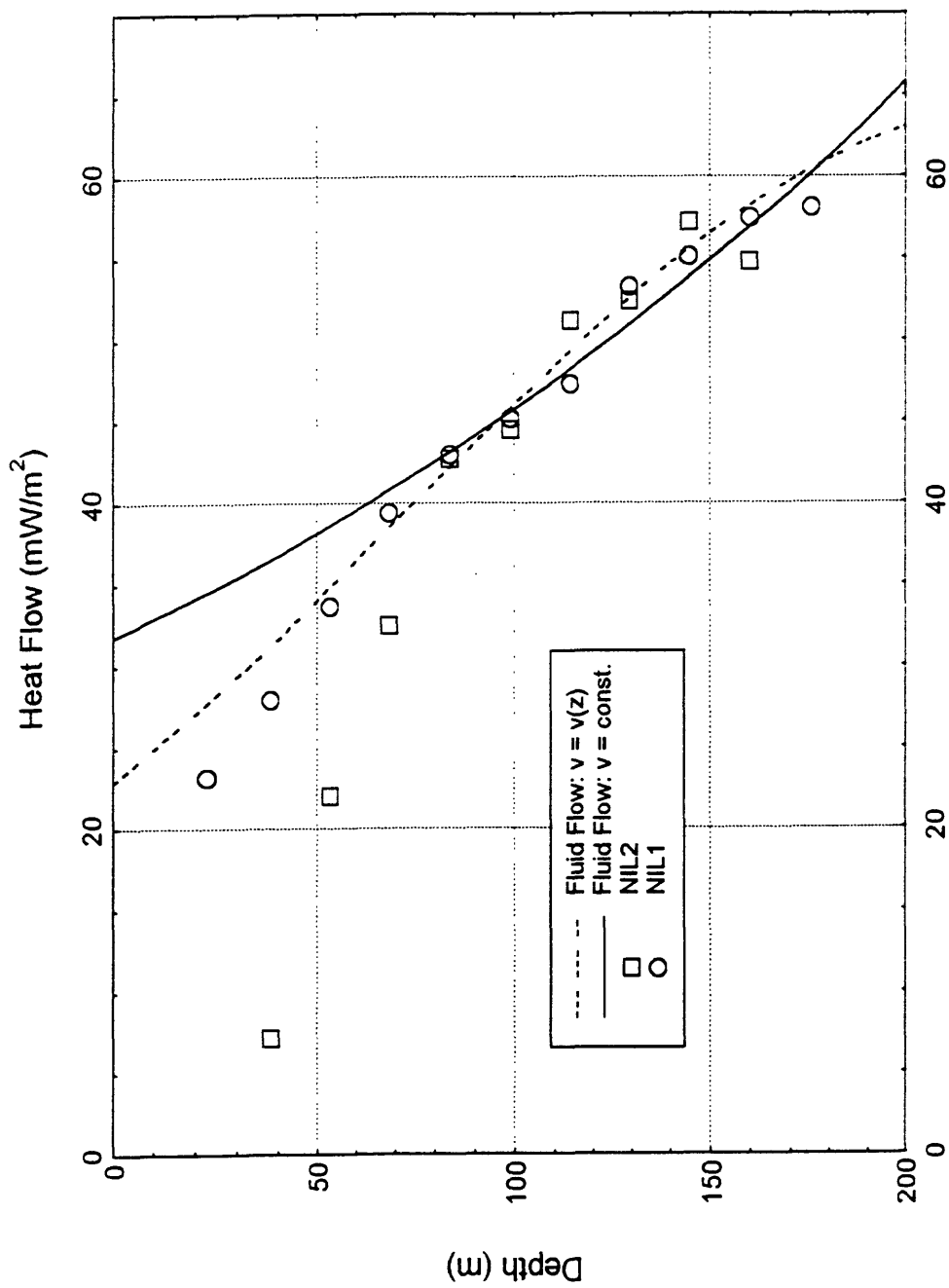
then the topographically-corrected gradients determined for the bottom sections of NIL1 and NIL2 in Table 6 should be close to the background value.

In the case of downward groundwater flow, the thermal disturbance is pervasive throughout the depth interval penetrated by the holes. If there is constant vertical groundwater flow from the surface ($z = 0$) at the Niles sites, the effect of this flow on measured heat flow is easily represented as

$$q(z) = q_0 \exp^{-zPe/L} \quad (4)$$

where q_0 is the apparent (i.e. measured) surface heat flow, L is the depth interval over which there is steady vertical groundwater flow, and Pe is the Peclet number, representing the ratio of advective to conductive heat flow (Clauser and Villinger, 1990). Figure 7 shows heat flow versus depth for NIL1 and NIL2 along with the best fit of Equation (4) to the combined data sets. The curve fit shown in Figure 7 results in $q_0 = 31.8 \text{ mW/m}^2$ and $Pe/L = -0.00364 \text{ m}^{-1}$. This provides a quantitative estimate of heat flow in all parts of the flow field for which the vertical groundwater flow rate is constant. In order to determine the appropriate depth at which to solve Equation (4) for the conductive heat flow below the groundwater flow (i.e. the background value) it is also necessary to estimate L .

The Niles sites are located approximately 400 meters above sea level, and it is reasonable to assume that L is greater than the drilled depth (180 meters) and less than the elevation. Niles Canyon has perennial stream flow from these locations approximately 300 meters below the drill sites. If we take 300 meters as the estimate for L , $q(300)$ is equal to 94.8 mW/m^2 . This value is highly sensitive to the choice of L and is almost certainly an upper bound on the background conductive heat flow. In reality, groundwater flow of this sort is not purely one-dimensional, even though the sites are located near the crest of the ridge. Water will tend to flow downslope, with a decreasing vertical component and an increasing horizontal component at greater depths. Even in constant velocity flow fields, the one-dimensional assumption breaks down at L because mass conservation requires that all of the fluid flow turn in a horizontal direction at this point.



Niles 1 and 2 Fluid Flow Models

Figure 7 - Heat flow versus depth for NIL1 (open circles) and NIL2 (open squares), along with best-fit curves for downward fluid flow that is constant with depth (solid line) and that is linearly-decreasing with depth (dashed line).

A more conservative (and perhaps more realistic) approach to the problem is to consider groundwater flow that decreases with depth down to L (i.e. $v(z) = v_0(z-L)/L$). In this model, the one-dimensional thermal nature of the problem is maintained by having horizontal flow along isotherms. Mass conservation is maintained by keeping the sum of vertical and horizontal transport constant. Application of this model (see Appendix) changes the dependence of heat flow with depth to

$$q(z) = q_0 \exp^{-(z-z^2/2L)Pe/L} \quad (5)$$

The advantages of this formulation are an independent solution for L separate from Pe and the maintenance of more realistic fluid and heat transport conditions at the base of the flow field. A curve-fit of this model to the combined data from NIL1 and NIL2 is shown in Figure 7 and provides $q_0 = 22.9 \text{ mW/m}^2$, $L = 232 \text{ m}$, and $Pe = -2.066$. At $z = L$, this leads to $q(L) = 64.4 \text{ mW/m}^2$.

There are limited data on which (if either) of the two possible processes, surface temperature change and groundwater flow, is actually taking place, but those data tend to favor a combination of the two in the upper 80 meters with groundwater flow predominating below 80 meters. If the observed curvature follows from changing surface temperature, then the change is limited to the Niles locality. There is no evidence for curvature of an equivalent magnitude and penetration depth at any of the other sites. The Coyote Hills temperature data show a similar curvature, but the thermal disturbance is limited to the upper 90 meters (see below). As far as groundwater flow is concerned, the pervasive fracturing observed in the core and televiwer logs is unique to the Niles and Sunol sites, and these are also sites with depressed geothermal gradients (see Sunol section below). In addition, the location of these sites near the top of relatively steep ridges places them at the point of greatest hydraulic potential for downward groundwater flow.

Consequently, the final heat flow values for these sites are presented using the two groundwater models outlined above. The applicability of these solutions is highly uncertain, so the final value is presented as an average of the two (80 mW/m^2) with an uncertainty of equal

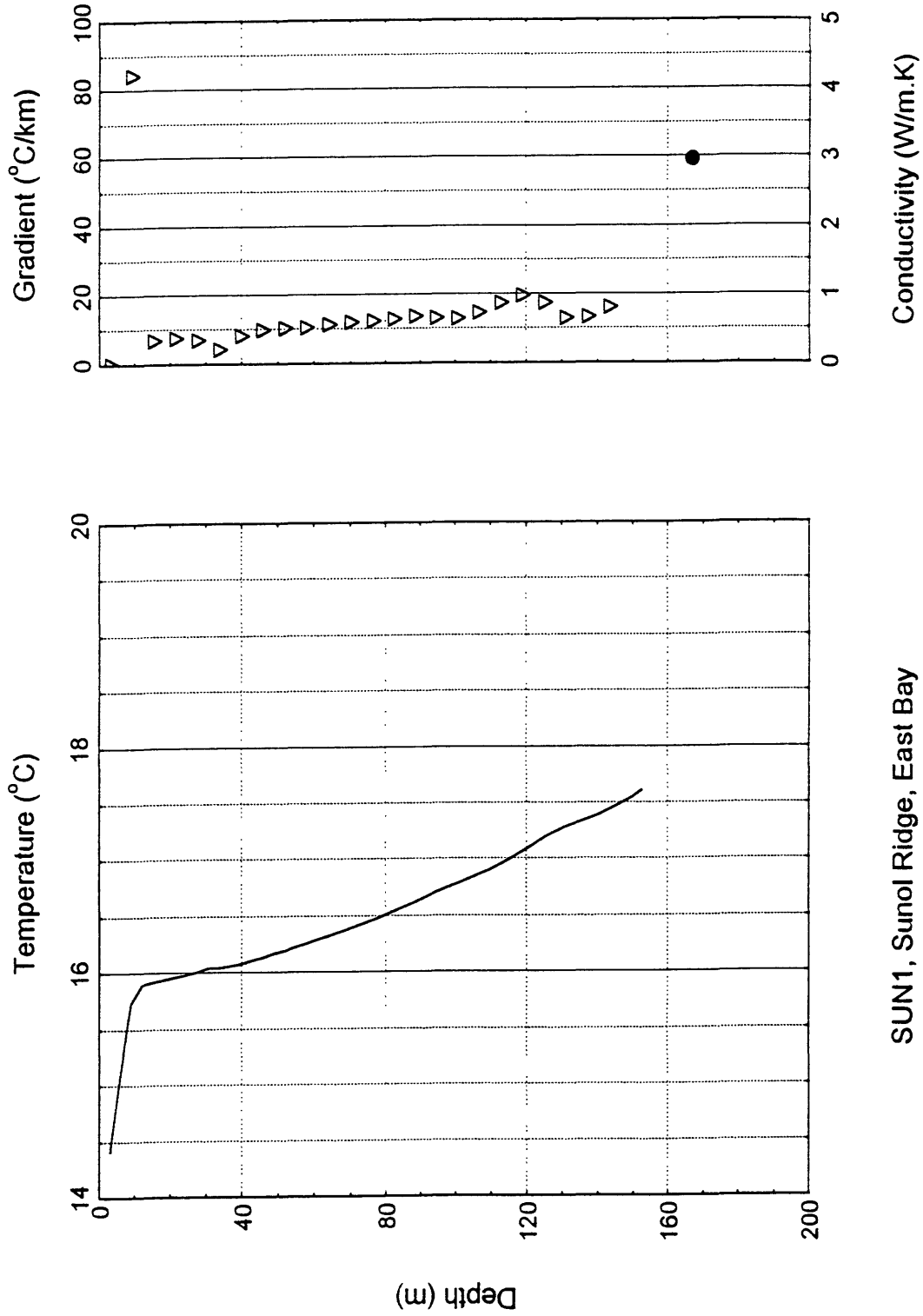
to the difference between the average and each model (± 15 mW/m²). Stated conservatively, groundwater flow at the Niles site results in an average heat flow, 58 mW/m², that is depressed relative the true background value. Simple, one-dimensional models for this flow suggest that this background value lies between 65 and 95 mW/m².

SUNOL RIDGE #1 (SUN1) -

This hole was drilled to a depth of 152 meters (500 feet) near the crest of Sunol Ridge approximately 3 km east of the Niles sites. As at the Niles site, drilling encountered an intensely fractured sandstone and shale sequence, with the fractures visible in both the recovered core and the televiwer log (J. Svitek, written comm., 1992). Subsurface temperatures, temperature gradients and thermal conductivity measured on a core sample are plotted in Figure 8. Below 40 meters, temperature gradients in SUN1 are variable in the range of 10 to 20 °C/km. The low gradients are probably due to downward groundwater flow, with the changes in value reflecting varying flow rates through individual fracture systems. Because the temperatures from SUN1 do not reveal the same systematic curvature with depth observed in NIL1 and NIL2, it was not possible to apply the Peclet number analysis to these data. Consequently, a heat flow value is not reported for the Sunol site.

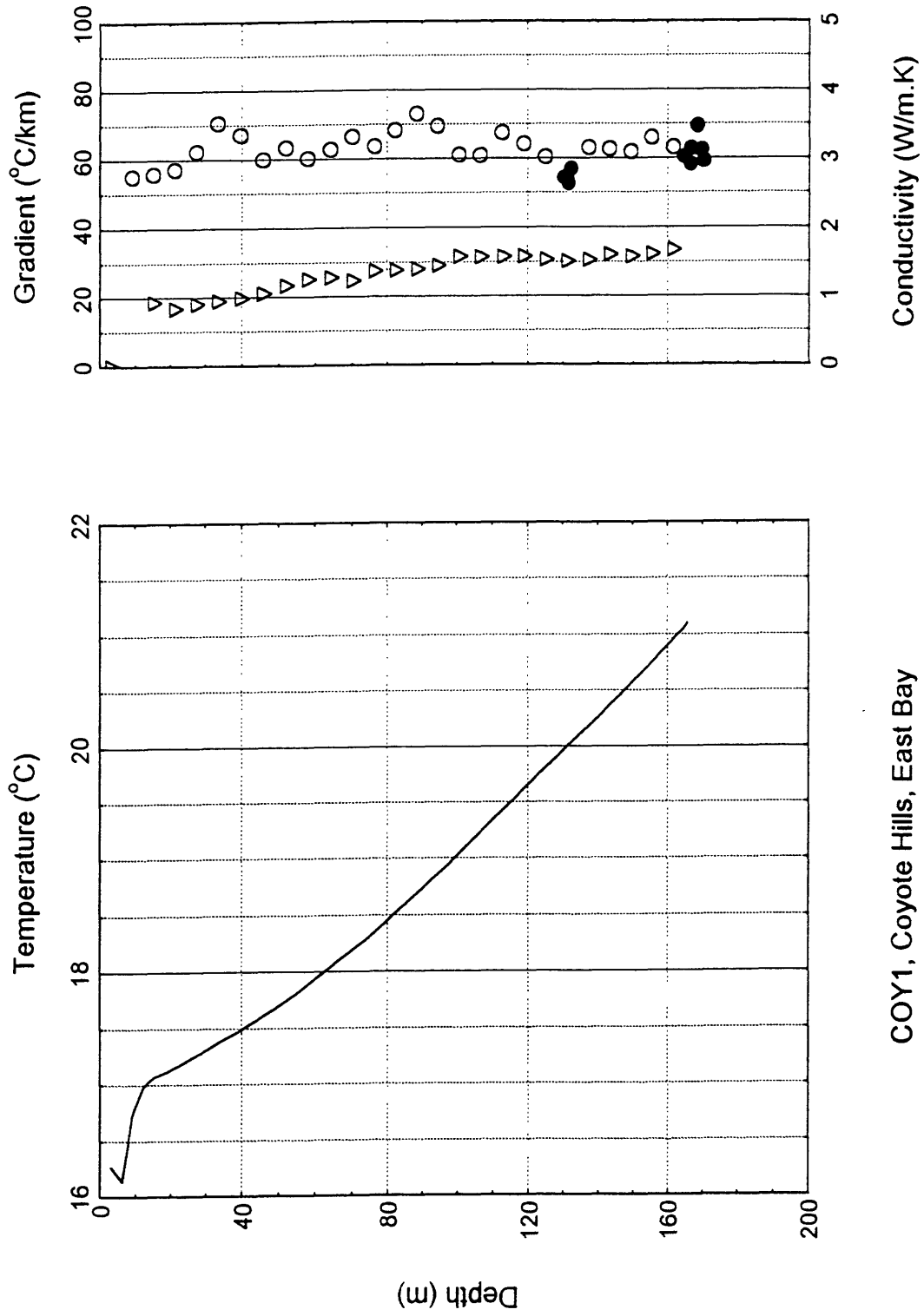
COYOTE HILLS #1 (COY1) -

This hole, located at the northern end of the Coyote Hills (Figure 1), was drilled to a depth of 560 feet in sandstone and argillite of the Franciscan Formation (Table 5; Snetsinger, 1976). The temperature profile from COY1 is curved upward in the upper 90 meters and linear below (Figure 9). This curvature most likely represents a response to surface temperature warming in the past few decades (see NILES section above). Unlike the heat flow in the Niles holes, heat flow in COY1 reaches a constant value at a depth of 90 meters and does not vary significantly down to the base of the hole (Figure 10). This is consistent with the thermal effects of a recent increase in surface temperature and is not consistent with downward groundwater flow. In addition, the maximum elevation in the Coyote Hills is less than 60 meters, with COY1 located at an elevation of 7 meters, leaving little potential for groundwater flow.



SUN1, Sunol Ridge, East Bay

Figure 8 - Temperature (solid line), vertical temperature gradient (open triangles), bulk thermal conductivity measured on core samples (solid circles) and bulk conductivity determined from cuttings samples (open circles) for SUN1.



COY1, Coyote Hills, East Bay

Figure 9 - Temperature (solid line), vertical temperature gradient (open triangles), bulk thermal conductivity measured on core samples (solid circles) and bulk conductivity determined from cuttings samples (open circles) for COY1.

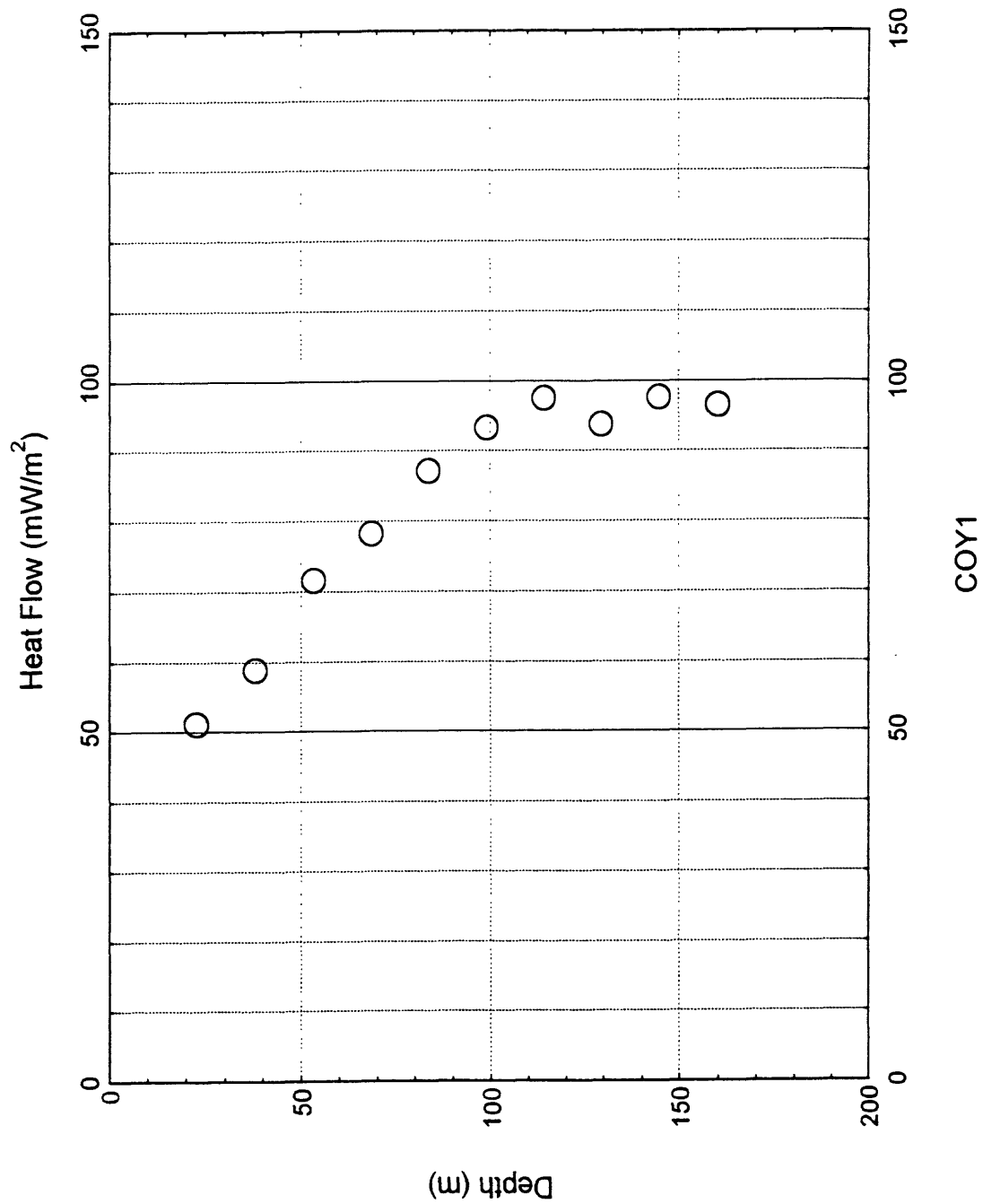


Figure 10 - Heat flow versus depth for COY1.

Gradients determined in the interval below 90 meters and thermal conductivities measured on cores and cuttings were combined to yield an average heat flow of 96.3 ± 1.4 mW/m², the most uniform value in the East Bay. High heat flow at Coyote Hills provides a direct tie between the high values measured on the San Francisco Peninsula and those in the hills east of the Hayward Fault.

CONCLUSIONS

Temperature and thermal conductivity data have been acquired from five strainmeter pilot holes and one strainmeter hole drilled near the Hayward fault. Although the locally rugged topography and associated groundwater flow disturb the geothermal gradient at most of the drillsites, four reliable conductive heat flow measurements have been obtained from holes at Lake Chabot (CHA1), Walpert Ridge (NIL1, NIL2), and Coyote Hills (COY1) (Figure 1).

The average heat flow from these three sites, along with a previously published value from the Berkeley Hills is 85.8 mW/m² with a standard deviation of 9.7 mW/m². This places the Hayward fault well within the Coast Range heat flow high, a region of elevated heat flow which roughly corresponds to the geomorphic expression of the Coast Ranges from the vicinity of Clear Lake in the north to the Transverse Ranges in the south (Lachenbruch and Sass, 1980). The data shown in Figure 11 do suggest a relatively abrupt decrease in heat flow to approximately 65 mW/m² just east of the Calaveras fault, but it is probably unwise to characterize the shape of this transition on the basis of a single measurement. Within the San Francisco Bay area, these new data are remarkably consistent with heat flow measured along the San Andreas fault on the San Francisco Peninsula (Figure 11). The six heat flow measurements on the San Francisco Peninsula average 89.2 mW/m² with a standard deviation of 9.7 mW/m². Given the small number of data points, this average is statistically indistinguishable from the 85.8 mW/m² average reported above for the Hayward fault region. This fact has important consequences for the nature of the San Andreas fault system in the San Francisco Bay area.

Recent models for the tectonic evolution of the Hayward and San Andreas faults (e.g. Furlong, 1993) suggest that the Pacific-North American plate boundary beneath the seismogenic layer is focused beneath the Hayward-Calaveras fault system and not under the San Andreas

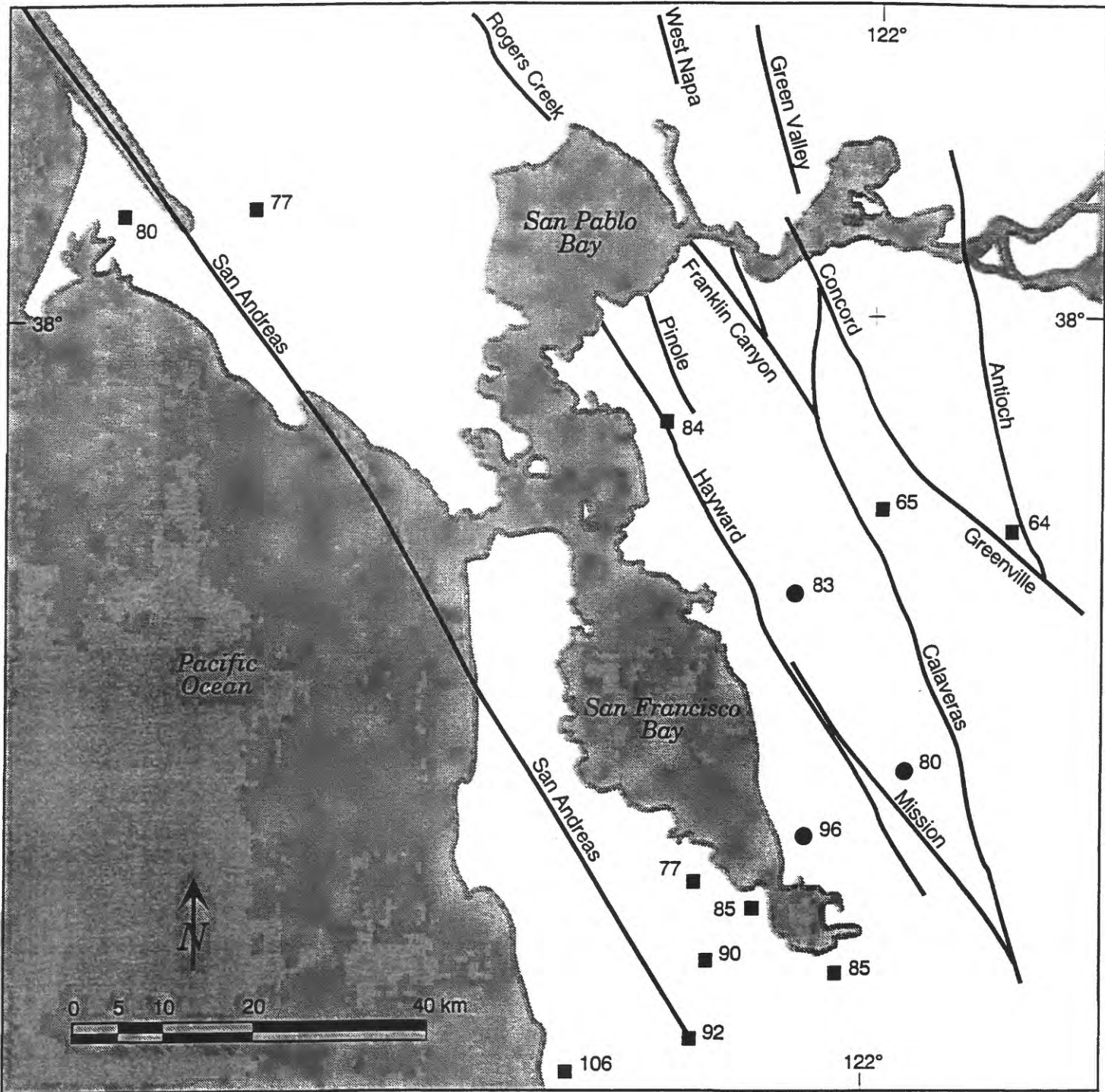


Figure 11 - Location map showing new heat-flow values along with published heat flow.

fault. According to the models of Furlong and others, this offset in the plate boundary at depth is due to asymmetric cooling of the sub-San Andreas lithosphere in the wake of the Mendocino Triple Junction. This modeled asymmetric cooling leaves the lithosphere beneath the Hayward fault weaker (i.e. hotter) and focuses the ductile part of the relative plate motion under this fault.

The heat flow data discussed above do not indicate that the lithosphere is substantially hotter under the Hayward fault than under the San Andreas fault, although it is possible that these surface heat flow measurements do not reflect current conditions at depth under these two fault systems. A static temperature change at a depth of 15 km (the approximate base of the seismogenic layer in the San Francisco Bay region) would not be reflected in surface heat flow until approximately 0.5 my had passed, and it would take approximately 2 my for heat flow to reach a new equilibrium value. However, the thickness of the seismogenic layer has a well-established sensitivity to changing thermal conditions, and earthquake focal depths on the San Andreas and Hayward faults are approximately the same (Hill et al., 1990). Consequently, the high heat flow values measured along the San Andreas and Hayward faults are most likely representative of relatively uniform and high temperatures at seismogenic and subseismogenic depths.

Table 1. Summary information for East Bay heat-flow holes

Hole name	Designation	Location (Lat., Long.)	Total depth (m)
Lake Chabot #1	CHA1	37°44.6'N, 122°5.7'W	151
Garin Park #2	GAR2	37°38.7'N, 122°0.6'W	156
Niles #1	NIL1	37°36.5'N, 121°57.9'W	184
Niles #2	NIL2	37°37.2'N, 121°58.6'W	168
Sunol Ridge #1	SUN1	37°39.2'N, 121°57.3'W	152
Coyote Hills #1	COY1	37°32.5'N, 122°5.7'W	170

Table 2. Lithologic data from Chabot #1 (CHA1)
based on analysis of core and cuttings

Depth (m)	Shale (%)	Sandstone (%)	Description
0	0	100	Oxidized zone; very fine to fine-grained (feldspathic wacke) sandstone; grains of quartz and feldspar are angular, trace of chloritized mica
6.1	0	100	
12.2	0	100	
18.3	0	100	
▼ Water Table - 21.3			
24.4	0	100	Fine to medium-grained, angular to subrounded clasts same composition as above.
30.5	0	100	
36.6	0	100	Trace of dark gray shale in zone 43-49m
42.7	0	100	
48.8	0	100	
54.9	0	100	
61.0	5	95	Minor dark gray shale appears; s.s. as above
67.1	5	95	Some s.s. and shale chunks are slickened 67-73m
73.2	5	95	Sandstone is medium to fine grained, light gray, massive
79.2	5	95	
85.3	5	95	
91.4	<10	>90	
97.5	<10	>90	
103.6	5	95	
109.7	5	95	
115.8	15	85	
121.9	20	80	
128.0	25	75	Driller thought he was hitting .6-.9m shale seams from 128-134m
134.1 to 140.2	30	70	134-140m more shaley than above
Cored 140.2-150.6			
140.2-140.4	<5	>95	Thin flat-bedded s.s. and dark shale thin interbeds
140.4-144.8	0	100	Massive s.s.
144.8-147.8	<5	>95	Massive s.s. (minor trough x-beds)
147.8-150.6	<5	>95	Dip 55° @ 148.3m and 149.2m; bituminous flakes @ 149.2m, thin matrix-supported layer of gravel [clasts well rounded to angular, composition mostly rhyolitic to dacitic (porphyry), also minor dark gray shale, clasts as large as 25 mm (avg. size ~5 mm)]

Table 3. Lithologic data from Niles #1 (NIL1)
based on analysis of core and cuttings

Depth (m)	Shale (%)	Sandstone (%)	Description
0	10	90	Oxidized zone; sandstone; medium to very fine grained (.25 - .06 mm)
6.1	10	90	lithic, feldspathic wacke, tan, trace pyrite
12.2	20	80	shale; tan to gray, fissile, some slickened
▼ Apparent Water Table			
18.3	25	75	Ss; fine to very fine grained, light gray
24.4	30	70	shale, medium to dark gray
30.5	0	100	Ss; medium to fine grained, light gray
36.6	30	70	Ss; fine to very fine grained, feldspathic wacke
42.7	30	70	shale, medium to dark gray
48.8	35	65	
54.9	15	85	Ss; medium to very fine, light gray feldspathic wacke; trace of pyrite;
61.0	15	85	some slickened-sides; shale; medium to dark gray
67.1	15	85	
73.2	15	85	Ss; medium grained, light gray feldspathic wacke, (cutting chunks fairly
79.2	10	90	large from - 76 - 85m, pieces equidimensional); shale, medium to dark
85.3	15	85	gray, massive
91.4	10	90	
97.5	20	80	
103.6	5	95	
109.7	5	95	
115.8	20	80	Ss and shale as above but now fragments are breaking into flake-shaped
121.9	20	80	pieces; more white vein material than in section above (may be more shear)
128.0	20	80	Shale; light to medium gray; massive ss; fine to very fine grained (white
134.1	30	70	earthy material in cuttings may be fault gouge)
140.2	30	70	
146.3	2	98	Ss; medium grained, light gray feldspathic wacke; shale, dark gray, massive
152.4 to 158.5	5	95	

Table 3. Lithologic data from Niles #1 (NIL1)
based on analysis of core and cuttings (continued)

Depth (m)	Shale (%)	Sandstone (%)	Description
Cored 158.5 – 184.4m			
158.5 – 161.4	5	95	Whole box is brecciated with fault gouge; 80% of ss is highly brecciated with angular fairly competent fragments in a matrix of fine-grained, earthy, lighter gray, mylonitized ss. Shears are pervasive and anastomosing (many dips range from 35° to 70°).
161.4 – 164.6			Lithologies as above
164.6 – 167.6	15	85	Lithologies as above
167.6 – 170.6	5	95	Shale is sheared and broken
170.6 – 173.6	5	95	Lithologies as above
173.6 – 176.8	<5	>95	Lithologies as above
176.8 – 179.8	<5	>95	Dip 45°; lithologies as above
179.8 – 182.9	<5	>95	Dip 45°; lithologies as above
182.9 – 184.4	30	70	Shale, very broken

Table 5. Lithologic data from Coyote Hills #1 (COY1)
based on analysis of core and cuttings

Depth (m)	Argillite (%)	Sandstone (%)	Description
0	20	80	Slightly oxidized; sandstone; fine-grained olive gray (5Y 3/2) graywacke
6.1	20	80	
12.2	30	70	Argillite; dark gray, sheared
18.3	5	95	Slightly oxidized; sandstone coarsens (fine to medium grained)
24.4	5	95	
30.5	10	90	
36.6	20	80	
42.7	30	70	More argillite than above
48.8	25	75	White CaCO ₃ veins in argillite
54.9	35	65	
61.0	40	60	
67.1	10	90	More ss than above
73.2	10	90	
79.2	25	75	
85.3	15	85	
91.4	10	90	
97.5	30	70	97.5m first appearance of reddish purple fine-grained material (sheared in argillite)
103.6	40	60	Cuttings are finer than above
109.7	45	55	
115.8	45	55	
121.9	50	50	
128.0	50	50	Tectonic fabric with 60-80° dip shears argillite and sandstone; white calcite veins
Cored 129.5 - 133m			
129.5-133	50	50	
134.1	40	60	
140.2	45	55	
146.3	40	60	
152.4	45	55	
158.5	45	55	
Cored 164.6 - 170.7m			
164.6-167.6	25	75	Tectonic fabric 60° - 80° dip shear
167.6-170.7	35	65	Argillite and sandstone with white calcite veins

Table 6. Summary of heat-flow determinations

Hole	Depth interval (m)	Temperature gradient ($^{\circ}\text{C}/\text{km}$) ¹	Thermal conductivity ($\text{W}/\text{m}\cdot\text{K}$) ²	Heat flow (mW/m^2)
CHA1	110—151	27.5±0.04	3.03±0.24	83.3±6.6
GAR2	140—148	29—49	2.88±0.08	80—140
NIL1	168—183	19.3±0.12	3.01±0.12	80±15(58.1) ³
NIL2	137—152	19.0±0.32	2.94±0.06	80±15(57.2) ³
COY1	76—168	31.1±0.04	3.10±0.08	96.3±2.5

¹Gradients are corrected for three-dimensional steady-state topography except GAR2, for which a range of approximate two-dimensional corrections were applied.

²Uncertainties in conductivity are 95% confidence limits.

³Value in parentheses is not corrected for fluid flow. Corrected value after Peclet number analysis is printed outside of parentheses.

APPENDIX

Thermal Effects of Vertical Groundwater Flow Rates Decreasing Linearly with Depth

The derivation of Equation 5 is a modification of the Bredehoeft and Papadopoulos (1965) Peclet number analysis that is similar to a thermal model developed by Lachenbruch et al. (1985) for sedimentation on extending crust. The conceptual model considers vertical ground water flow that can be characterized as $v(z) = v_0(z-L)/L$, where v_0 is the downward fluid velocity at the surface $z = 0$ and L is the thickness of the layer through which this vertical flow occurs. To maintain conservation of mass, the decrease of vertical flow with depth is compensated by a balancing horizontal flow. In order for the thermal effects of this two-dimensional flow system to be solvable with one-dimensional analytical model, it is assumed that all of the horizontal flow is directed along isotherms and that the flow system has reached steady state. This is likely to be a poor assumption at downslope locations where isotherms will tend to follow the sloping ground surface but is applicable to ridge tops where isotherms will be subhorizontal. This model should be applicable to the Niles sites, which are located near the crest of Walpert Ridge.

For simplicity, the following boundary conditions are applied. At $z=0$, $T=0$ and $v=v_0$. At $z=L$, $T=T_L$ and $v=0$. The relevant heat transport equation is

$$\frac{d}{dz} \cdot \left(\lambda \frac{dT}{dz} \right) = -\rho_f c_f v(z) \frac{dT}{dz} \quad (\text{A1})$$

where λ is the thermal conductivity, ρ_f is the fluid density, c_f is the heat capacity, and $v(z)$ is defined as $v_0(z-L)/L$. Equation A1 can be reduced to a non-dimensional form by setting $\xi = z/L$, $\Theta = T/T_L$, and defining the Peclet number as $Pe = \rho_f c_f v_0 L / \lambda$. This simplifies the above equation to

$$\frac{d^2 \Theta}{d\xi^2} = -Pe(\xi - 1) \frac{d\Theta}{d\xi} \quad (\text{A2})$$

with the boundary conditions that at $\xi=0$, $\Theta=0$ and at $\xi=1$, $\Theta=1$. The complete solution to

this is

$$\Theta = \frac{\operatorname{erf}\left(\sqrt{\frac{Pe}{2}}(\xi - 1)\right) + \operatorname{erf}\left(\sqrt{\frac{Pe}{2}}\right)}{\operatorname{erf}\left(\sqrt{\frac{Pe}{2}}\right)} \quad (\text{A3})$$

For this study, the measurement of interest is heat flow, which can be found by defining a dimensionless temperature gradient, $p = d\Theta/d\xi$. The derivative of Equation A3 yields

$$p = \frac{e^{-\frac{Pe}{2}(\xi-1)^2}}{\sqrt{\frac{\pi}{2Pe}} \operatorname{erf}\left(\sqrt{\frac{Pe}{2}}\right)} \quad (\text{A4})$$

which reduces to the thermal gradient portion of Equation 5 when dimensional variables are substituted.

REFERENCES

- Birch, F., 1950, Flow of heat in the Front Range, Colorado: *Bull. Geol. Soc. Amer.*, v. 61, p. 567-620.
- Bredehoeft, J.D., and Papadopoulos, I.S., 1965, Rates of vertical groundwater movement estimated from the Earth's thermal profile, *Water Resour. Res.*, v. 1, no. 2, p. 325-328.
- Clauser, C., and Villinger, H., 1990, Analysis of conductive and convective heat transfer in a sedimentary basin, demonstrated for the Rhinegraben, *Geophys. J. Int.*, v. 100, p. 393-414.
- Dibblee, T.W., Jr., 1980a, Preliminary geologic map of the Hayward Quadrangle, Alameda and Contra Costa Counties: *U.S. Geological Survey Open-File Report 80-540*.
- Dibblee, T.W., Jr., 1980b, Preliminary geologic map of the Niles Quadrangle, Alameda County: *U.S. Geological Survey Open-File Report 80-533C*.
- Furlong, K.P., 1993, Thermal-rheologic evolution of the upper mantle and the development of the San Andreas fault system: *Tectonophysics*, v. 223, p. 149-164.
- Hill, D.P., Eaton, J.P., and Jones, L.M., 1990, Seismicity, 1980-86: in Wallace, R.E., The San Andreas fault system, *U.S. Geological Survey Prof. Paper 1515*, 283 p.
- Johnston, M.J.S., Myren, G.D., Linde, A.J., and Gladwin, M.J., 1992, A focused earthquake prediction experiment on the Hayward Fault; array plans and expected strains and displacements for rupture of the southern segment: in Galehouse, J.S., 2nd Conference on earthquake hazards in the eastern San Francisco Bay area: *Calif. Div. Mines and Geol. Spec. Pub.*, v. 62, p. 34.

- Lachenbruch, A.H., 1969, The effect of two-dimensional topography on superficial thermal gradients: *U.S. Geological Survey Bulletin 1203-E*, 86 p.
- Lachenbruch, A.H., and Marshall, B.V., 1986, Changing climate: geothermal evidence from permafrost in the Alaskan Arctic: *Science*, v. 234, p. 689-696.
- Lachenbruch, A.H., and Sass, J.H., 1980, Heat flow and energetics of the San Andreas fault zone: *J. Geophys. Res.*, v. 85, n. B11, p. 6185-6222.
- Lachenbruch, A.H., Sass, J.H., and Galanis, S.P., Jr., 1985, Heat flow in southernmost California and the origin of the Salton Trough: *J. Geophys. Res.*, v. 90, n. B8, p. 6709-6736.
- Moses, T.H., Jr., and Sass, J.H., 1979, Drilling techniques presently in use by the Geothermal Studies Project, U.S. Geological Survey: *U.S. Geological Survey Open-File Report 79-763*, 26 p.
- Sass, J.H., Lachenbruch, A.H., and Munroe, R.J., 1971, Thermal conductivity of rocks from measurements on fragments and its application to heat-flow determinations, *J. Geophys. Res.*, v. 76, p. 3391-3401.
- Sass, J.H., Lachenbruch, A.H., Munroe, R.J., Greene, G.W., and Moses, T.H., Jr., 1971, Heat flow in the western United States, *J. Geophys. Res.*, v. 76, p. 6376-6413.
- Snetsinger, K.G., 1976, Rock types of the Franciscan Formation, Coyote Hills, Alameda County, California: *California Geology*, v. 29, n. 8, p. 174-177.